Calcification in Three Common Calcified Algae from Phuket, Thailand: Potential Relevance on Seawater Carbonate Chemistry and Link to Photosynthetic Process

Pimchanok Buapet [1,2] and Sutinee Sinutok [2,3,*]

[1] Division of Biological Science, Faculty of Science, Prince of Songkla University, Hat Yai 90110, Songkhla, Thailand; pimchanok.b@psu.ac.th
[2] Coastal Oceanography and Climate Change Research Center, Prince of Songkla University, Hat Yai 90110, Songkhla, Thailand
[3] Faculty of Environmental Management, Prince of Songkla University, Hat Yai 90110, Songkhla, Thailand
[*] Correspondence: sutinee.s@psu.ac.th; Tel.: +66-(0)-7428-6847

Abstract: Calcifying macroalgae contribute significantly to the structure and function of tropical marine ecosystems. Their calcification and photosynthetic processes are not well understood despite their critical role in marine carbon cycles and high vulnerability to environmental changes. This study aims to provide a better understanding of the macroalgal calcification process, focusing on its relevance concerning seawater carbonate chemistry and its relationship to photosynthesis in three dominant calcified macroalgae in Thailand, *Padina boryana*, *Halimeda macroloba* and *Halimeda opuntia*. Morphological and microstructural attributes of the three macroalgae were analyzed and subsequently linked to their calcification rates and responses to inhibition of photosynthesis. In the first experiment, seawater pH, total alkalinity and total dissolved inorganic carbon were measured after incubation of the macroalgae in the light and after equilibration of the seawater with air. Estimations of carbon uptake into photosynthesis and calcification and carbon release into air were obtained thereafter. Our results provide evidence that calcification of the three calcified macroalgae is a potential source of CO_2, where calcification by *H. opuntia* and *H. macroloba* leads to a greater release of CO_2 per biomass weight than *P. boryana*. Nevertheless, this capacity is expected to vary on a diurnal basis, as the second experiment indicates that calcification is highly coupled to photosynthetic activity. Lower pH as a result of inhibited photosynthesis under darkness imposes more negative effects on *H. opuntia* and *H. macroloba* than on *P. boryana*, implying that they are more sensitive to acidification. These effects were worsened when photosynthesis was inhibited by 3-(3,4-dichlorophenyl)-1,1-dimethylurea, highlighting the significance of photosynthetic electron transport-dependent processes. Our findings suggest that estimations of the amount of carbon stored in the vegetated marine ecosystems should account for macroalgal calcification as a potential carbon source while considering diurnal variations in photosynthesis and seawater pH in a natural setting.

Keywords: blue carbon; climate change; macroalgae; ecophysiology

1. Introduction

Since the mid-18th century, atmospheric CO_2 has risen from 280 to 400 ppm, and is predicted to increase to 730–1200 ppm by 2100 as a result of human activities, such as the burning of fossil fuel, deforestation, agriculture and industrialization [1,2]. This has led to an increase in sea-surface temperature (ocean warming) and a decrease in ocean pH (ocean acidification), which have affected a range of marine floras and faunas [3–5]. Macroalgae play important roles as primary producers in the marine food chain and serve as habitat for various animals, which directly contribute to the livelihood and food security of the coastal community [6,7]. Recent studies have suggested that macroalgae may play a role in carbon sequestration, thus mitigating the changing climate, and offset anthropogenic carbon emissions to the atmosphere [8–11].

Calcifying macroalgae are intriguing organisms and have become a subject of interest for recent marine frontiers research [12–15] as they are a source of primary production via photosynthesis as well as $CaCO_3$ production via calcification with relatively fast growth and turnover rates compared to corals [16,17]. However, their role in the carbon economy, whether they act as a net sink or source of carbon, remains a knowledge gap and debatable [18–20] mainly due to uncertainties about the fate of carbon associated with calcification. Previous studies suggest that in the pathway of calcification, the chemical reaction step modifies the carbonate chemistry of the seawater and releases CO_2, resulting in a net loss of CO_2 to the atmosphere [18,21–23]. A recent study by Kalokora et al. [20] found that calcification in a calcifying alga, *Corallina officinalis* L., can release a significant amount of CO_2 to the atmosphere and become a source of CO_2 if not refixed via photosynthesis in the system, highlighting the complex role of algal calcification on carbon capture potential in coastal areas [20].

Calcification is closely coupled to photosynthesis because photosynthetic carbon uptake decreases CO_2, elevates pH and increases the CO_3^{2-} proportion in the carbonate–bicarbonate system of the seawater, which promotes $CaCO_3$ precipitation [24–28]. Respiratory CO_2 release takes place in darkness, lowering seawater pH and promoting $CaCO_3$ dissolution [13,29]. This relationship may change partly due to interspecific variations in the mechanisms and efficiency of photosynthetic carbon acquisition [30,31] and in the capacity to regulate the pH in the microenvironment [28,30–32]. A balance between all these simultaneous and interrelated processes partly shapes the daily and seasonal variations in calcification rates and carbon flux of shallow coastal water [26,33].

Species from genera *Padina* and *Halimeda* are calcifying macroalgae from divisions Phaeophyta and Chlorophyta commonly found in coastal subtropical and tropical habitats, including in Thailand [8,32,34,35]. While species from genus *Halimeda* have long been a model for calcification investigation, much less is known about species from genus *Padina*. *Padina* deposits aragonite crystals at cell surface, whereas *Halimeda* precipitates $CaCO_3$ in the form of aragonite in intercellular spaces [36–39]. The source of $CaCO_3$ for calcification of *Padina* is, thus, in the surface seawater layer on the thalli, whereas that of *Halimeda* is in the calcification fluid in interutricular spaces [36–39]. The species from genus *Padina* was categorized as lightly calcified where $CaCO_3$ ranged from 9% to 63%, 21% and 38% of dry weight in *Padina pavonica*, *Padina japonica* and *Padina sanctae-crucis*, respectively [37,40,41], while the species from genus *Halimeda* has greater $CaCO_3$ precipitation (81% and 86% of dry weight in *H. macroloba* and *H. cylindracea*, respectively [27]). Differential degrees of calcification and variation in microstructures are expected to be linked with their carbon use, particularly how they modify seawater chemistry and their carbon economy. In addition, the diversity of calcification sites and their proximity to pH-elevating processes (e.g., photosynthesis, H^+ pumping and carbon concentrating mechanisms (CCMs)) relative to external seawater might affect their response to changing environments [14,28,39,42,43].

This study aims to provide a better understanding of the calcification process, focusing on its role in carbon economy and its relationship to photosynthesis in three dominant calcified macroalgae in upper sublittoral areas in Phuket, Thailand, *P. boryana*, *H. opuntia* and *H. macroloba* [44–47]. Our findings will improve estimations on the amount of carbon stored in the vegetated marine ecosystems and support the evidence-based management on mitigating the impact of human-induced climate change.

2. Results

Specific thallus area (wet weight) of *P. boryana*, *H. opuntia* and *H. macroloba* were 37.09 ± 1.83, 6.41 ± 0.28 and 6.31 ± 0.40 cm^2 g^{-1}, respectively, while the specific thallus area (dry weight) of *P. boryana*. *H. opuntia* and *H. macroloba* were 163.88 ± 13.37, 14.84 ± 1.32 and 23.97 ± 1.50 cm^2 g^{-1}, respectively. Specific thallus area (wet and dry weight) of *P. boryana* was significantly greater than that of *H. opuntia*, and *H. macroloba* (Fisher's LSD test, $p < 0.001$ and $p < 0.001$, respectively). $CaCO_3$ in the form of aragonite of *P. boryana*, *H. opuntia* and *H. macroloba* were 46.89 ± 3.57, 81.44 ± 1.71 and $77.35\% \pm 1.44\%$ dry weight,

respectively, suggesting that *H. opuntia* and *H. macroloba* had greater $CaCO_3$ precipitation than *P. boryana* (Fisher's LSD test, $p < 0.001$ and $p < 0.001$, respectively), with no significant difference in %$CaCO_3$ between *H. opuntia* and *H. macroloba* ($p = 0.246$). $CaCO_3$ crystals of *P. boryana* were precipitated at the cell surface, whereas *H. opuntia* and *H. macroloba* precipitate $CaCO_3$ in intercellular spaces. Figure 1 shows locations of primary utricles (pU), primary interutricle spaces (pIUS) and aragonite crystals of *H. opuntia* and *H. macroloba* and cellular structure and aragonite crystals of *P. boryana*. Aragonite crystals of *P. boryana*, *H. opuntia* and *H. macroloba* were needle- or rod-shaped and were 0.13 ± 0.02, 0.22 ± 0.02 and 0.12 ± 0.02 μm wide and 1.36 ± 0.05, 1.80 ± 0.09 and 1.24 ± 0.05 μm long, respectively (Figure 1). Significant longer and wider aragonite crystals were observed in *H. opuntia* (Fisher's LSD test, $p < 0.001$ and $p < 0.001$, respectively). The $CaCO_3$ crystal densities of *P. boryana*, *H. opuntia* and *H. macroloba* were 5.26 ± 0.41, 3.47 ± 0.12 and 5.65 ± 0.34 needles μm^{-2}, respectively (Table 1). *H. opuntia* had significantly lower crystal density than *P. boryana* and *H. macroloba* (Fisher's LSD test, $p < 0.001$).
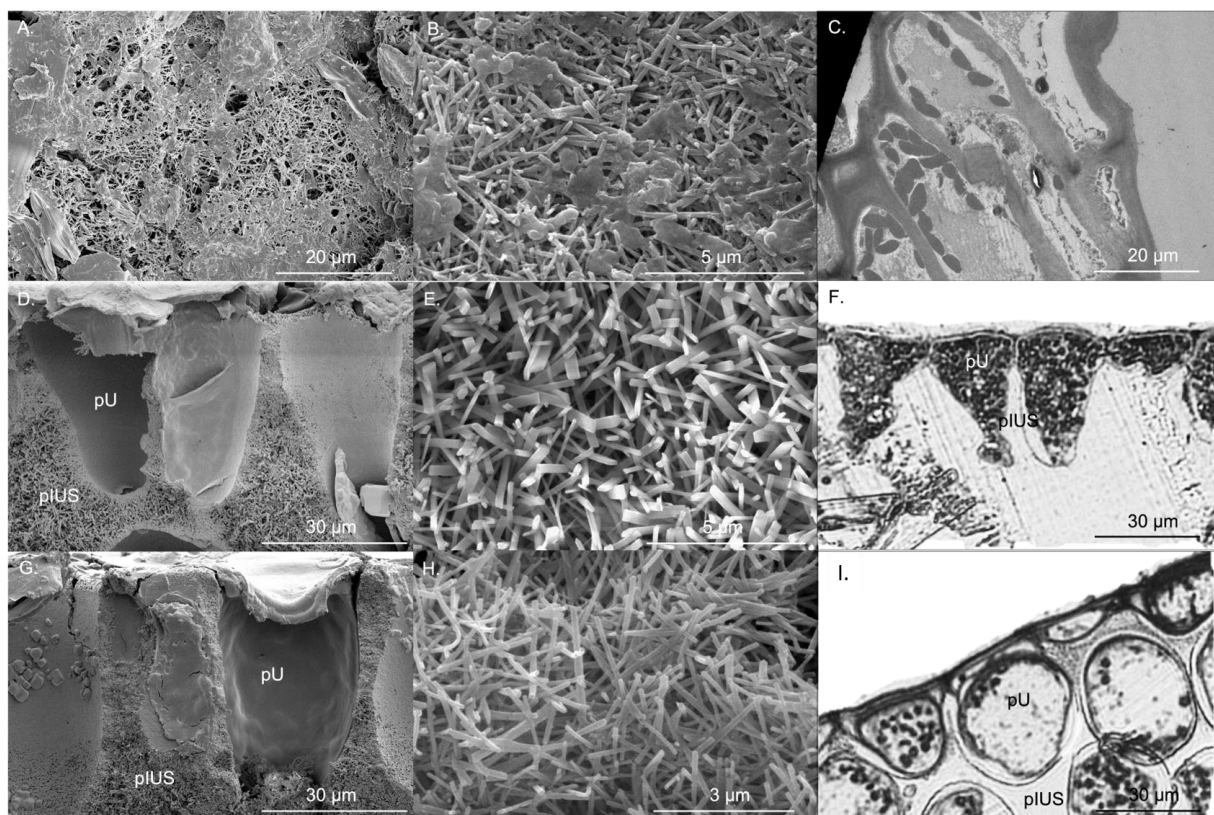

Figure 1. Aragonite crystal microstructure of *Padina boryana* (**A**,**B**), *Halimeda opuntia* (**D**,**E**) and *Halimeda macroloba* (**G**,**H**) from scanning electron microscope, cell of *P. boryana* (**C**), primary utricle (pU) and primary interutricle spaces (pIUS) of *H. opuntia* (**F**) and *H. macroloba* (**I**) from transmission electron microscope and compound microscope.

Table 1. Morphological and anatomical characters of *Padina boryana*, *Halimeda opuntia* and *Halimeda macroloba*. Data are Mean $\pm$ SE. Different uppercase letters indicate statistical difference (Fisher's LSD test, $p < 0.05$).

	Padina boryana	*Halimeda opuntia*	*Halimeda macroloba*
Specific thallus area (cm^2 g^{-1} fw)	37.09 ± 1.83 [a]	6.41 ± 0.28 [b]	6.31 ± 0.40 [b]
Specific thallus area (cm^2 g^{-1} dw)	163.88 ± 13.37 [a]	14.84 ± 1.32 [b]	23.97 ± 1.50 [b]
% Dry weight of calcium carbonate	46.89 ± 3.57 [a]	81.44 ± 1.71 [b]	77.35 ± 1.44 [b]
Calcium carbonate polymorph	Aragonite	Aragonite	Aragonite
Site of calcium carbonate	Cell surface	Intercellular spaces	Intercellular spaces

Table 1. *Cont.*

	Padina boryana	*Halimeda opuntia*	*Halimeda macroloba*
Calcium carbonate crystal shape	Needle or rod shape	Needle or rod shape	Needle or rod shape
Crystal width (μm)	0.13 ± 0.02 [a]	0.22 ± 0.02 [b]	0.12 ± 0.02 [a]
Crystal length (μm)	1.36 ± 0.05 [a]	1.80 ± 0.09 [b]	1.24 ± 0.05 [a]
Crystal density (needles μm^{-2})	5.26 ± 0.41 [a]	3.47 ± 0.12 [b]	5.65 ± 0.34 [c]
Surface diameter of primary utricle (μm)	-	23.67 ± 0.69 [a]	28.31 ± 0.40 [b]
Diffusion pathway length (μm)	-	5.95 ± 0.25 [a]	22.11 ± 0.51 [b]

[a, b, c] Significant difference.

The surface diameter of primary utricles (pU) of *H. macroloba* (28.31 ± 0.40 μm) was significantly larger than that of *H. opuntia* (23.67 ± 0.69 μm) (*t*-test, $p < 0.001$), while the diffusion pathway length of *H. macroloba* (22.11 ± 0.51 μm) was almost four-fold larger than that of *H. opuntia* (5.95 ± 0.25 μm) (*t*-test, $p < 0.001$) (Table 1).

The biological processes of the three macroalgae incubated in the light presented changes in seawater carbonate chemistry (Figure 2, Table 2). No significant alteration in controls (seawater without macroalgae) confirmed that the observed change in other treatments was associated with biological processes. Repeated-measures ANOVA showed that macroalgal species ($p < 0.001$), time of measurements (initial, after 3 h in the light and after equilibration with air, $p < 0.001$) and an interaction of the two factors ($p < 0.001$) significantly affected seawater pH, TA and total DIC (Figure 2). After exposure to the light for 3 h, a significant increase in seawater pH was detected in incubated *P. boryana* (reaching 8.79 ± 0.15, Fisher's LSD test, $p < 0.05$), a reduction in seawater pH was detected in incubated *H. opuntia* (Fisher's LSD test, $p < 0.05$) and no significant change in seawater pH compared to the initial values was observed in incubated *H. macroloba* (Figure 2A). Seawater pH was restored to the initial level after *P. boryana* was removed and the seawater was allowed to be equilibrated with air. In contrast, seawater pH remained low in treatment with *H. opuntia* (Fisher's LSD test, $p < 0.05$ compared to the initial value) and reduced in treatment with *H. macroloba* (Fisher's LSD test, $p < 0.05$). A significant decrease in TA was detected in the seawater incubated with all species tested after light exposure (Fisher's LSD test, $p < 0.05$, Figure 2B). After equilibration, a recovery of TA was observed in treatment with *P. boryana*, whereas TA in the other two treatments remained low. Total DIC followed the same trend as observed in TA (Figure 2C). These shifts in pH and TA resulted in a change in CO_2, HCO_3^-, CO_3^{2-}, saturation of calcite (ΩCa) and saturation of aragonite (ΩAr) (Table 2). Incubation of *P. boryana* in the light resulted in a decrease in CO_2 and HCO_3^- and an increase in CO_3^{2-}, ΩCa and ΩAr in seawater (Fisher's LSD test, $p < 0.05$). After equilibration, CO_2 and HCO_3^- were restored to the initial levels, whereas CO_3^{2-} ΩCa and ΩAr in the seawater became slightly lower than the initial values (Table 2, Fisher's LSD test, $p < 0.05$). The incubation of *H. opuntia* and *H. macroloba* displayed similar responses. After light exposure, all parameters were reduced (Fisher's LSD test, $p < 0.05$) except for CO_2, which showed an increase in *H. opuntia* (Fisher's LSD test, $p < 0.05$) and a slight decrease from the initial value, although not statistically significant in *H. macroloba*. Equilibration reinstated CO_2 concentration but did not restore HCO_3^- CO_3^{2-} ΩCa and ΩAr (Table 2, Fisher's LSD test, $p < 0.05$). The salinity and temperature of the seawater remained steady throughout the experiments (30 ppt; 30 °C–31 °C).
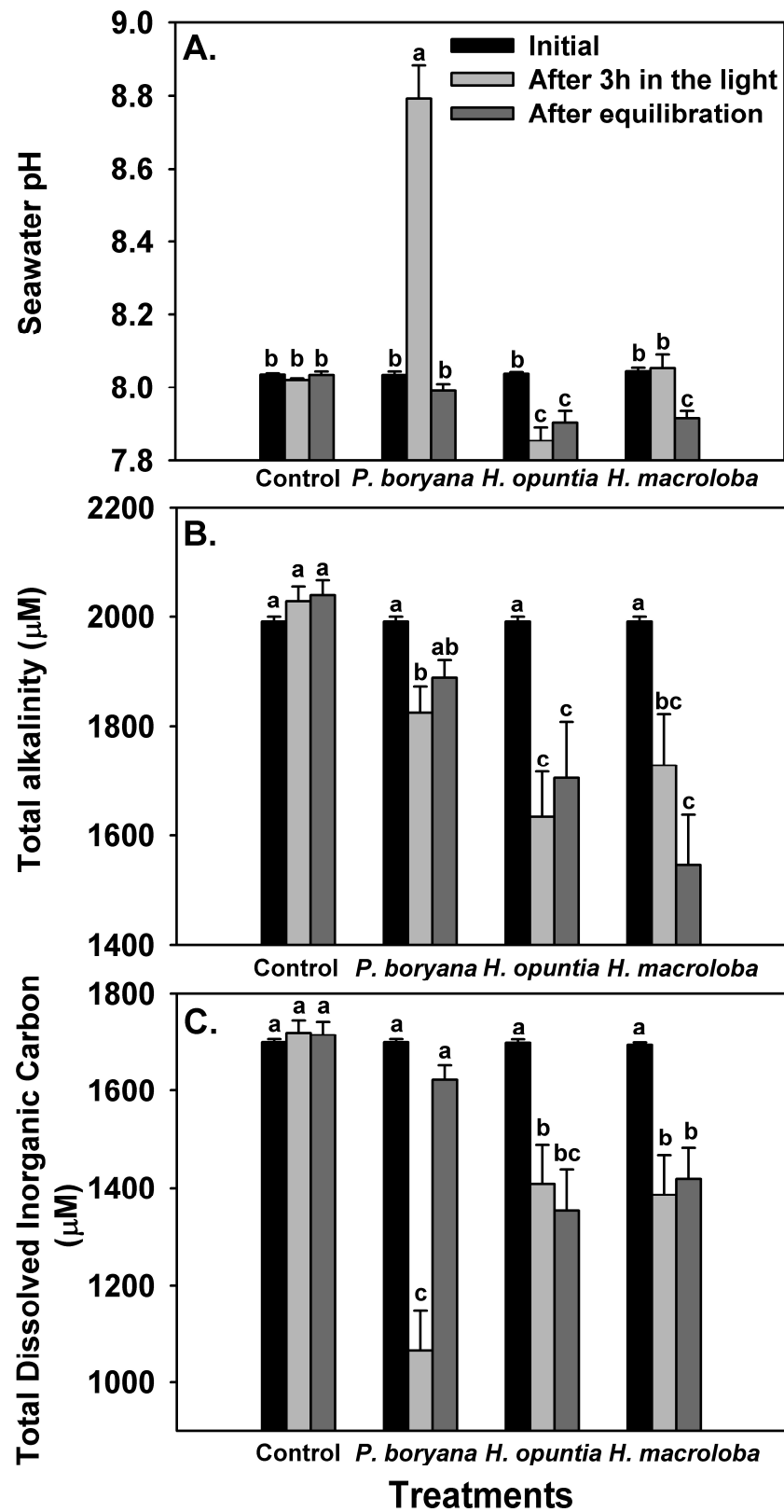
Figure 2. Changes in seawater chemistry: pH (**A**), total alkalinity (**B**) and total dissolved inorganic carbon (**C**) after incubation with *Padina boryana*, *Halimeda opuntia* and *Halimeda macroloba* under an irradiance of 150 μmol photons m^{-2} s^{-1} and after equilibration with air. The same set-up without macroalgae serves as the control. Bars without shared letters are considered statistically different (Fisher's LSD test, $p < 0.05$). Data are means ± SE (n = 9).

Table 2. A summary of seawater carbonate chemistry before an incubation with *Padina boryana*, *Halimeda opuntia* and *Halimeda macroloba* (initial), after 3 hours of incubation and after equilibration with air. The values presented were calculated from the average total alkalinity and pH (see Figure 2) using CO_2 sys.xls program (version 2.3). Data are means $\pm$ SE (n = 9). Different uppercase letters indicate statistical difference (Fisher's LSD test, $p < 0.05$).

DIC	*Padina boryana*		
	Initial	After 3 h Incubation	After Equilibration
CO_2 (μM)	8.97 ± 0.22 [a]	0.93 ± 0.26 [b]	9.64 ± 0.51 [a]
HCO_3^- (μM)	1491.83 ± 6.64 [a]	628.83 ± 93.61 [b]	1438.83 ± 28.28 [a]
CO_3^{2-} (μM)	199.57 ± 3.80 [a]	436.15 ± 20.38 [b]	174.50 ± 6.66 [c]
ΩCa	4.97 ± 0.09 [a]	10.88 ± 0.50 [b]	4.35 ± 0.16 [a]
ΩAr	3.31 ± 0.06 [a]	7.24 ± 0.33 [b]	2.89 ± 0.11 [c]
DIC	*Halimeda opuntia*		
	Initial	After 3 h Incubation	After Equilibration
CO_2 (μM)	8.86 ± 0.10 [a]	12.12 ± 1.41 [c]	9.85 ± 0.56 [a]
HCO_3^- (μM)	1489.30 ± 6.19 [a]	1281.85 ± 73.01 [c]	1217.81 ± 71.85 [c]
CO_3^{2-} (μM)	200.56 ± 2.16 [a]	114.93 ± 9.95 [d]	125.61 ± 14.61 [d]
ΩCa	5.00 ± 0.05 [a]	2.86 ± 0.24 [d]	3.13 ± 0.36 [d]
ΩAr	3.33 ± 0.03 [a]	1.90 ± 0.16 [d]	2.08 ± 0.24 [d]
DIC	*Halimeda macroloba*		
	Initial	After 3 h Incubation	After Equilibration
CO_2 (μM)	8.71 ± 0.40 [ad]	7.29 ± 0.81 [d]	9.50 ± 0.25 [a]
HCO_3^- (μM)	1483.06 ± 4.73 [a]	1210.38 ± 75.68 [c]	1276.53 ± 53.11 [c]
CO_3^{2-} (μM)	203.04 ± 3.97 [a]	168.60 ± 11.24 [ac]	132.38 ± 10.27 [d]
ΩCa	5.06 ± 0.09 [a]	4.20 ± 0.28 [c]	3.30 ± 0.25 [d]
ΩAr	3.37 ± 0.06 [a]	2.80 ± 0.18 [c]	2.19 ± 0.17 [c]

[a,b,c,d] Significant difference.

Fates of the DIC associated with biological processes differed among species (Figure 3). Photosynthetic carbon uptake was highest in *P. boryana* (Fisher's LSD test, $p < 0.05$), whereas *H. opuntia* and *H. macroloba* displayed comparable rates (Figure 3A), corroborating the pH drift and DIC results previously described in Figure 2 and Table 2. Opposite trends were observed in carbon removal by calcification and carbon loss due to biological processes (Figure 3B,C). The amount of carbon associated with both processes was lowest in *P. boryana* (Fisher's LSD test, $p < 0.05$), whereas no difference was detected between *H. opuntia* and *H. macroloba*. With lightly calcified algae, *P. boryana* was more engaged in photosynthetic carbon uptake than in calcification, resulting in no net carbon loss. In contrast, two heavily calcified macroalgae removed a larger amount of carbon for calcification than for photosynthesis. The consequential carbon loss was almost as high as their carbon removal for calcification.
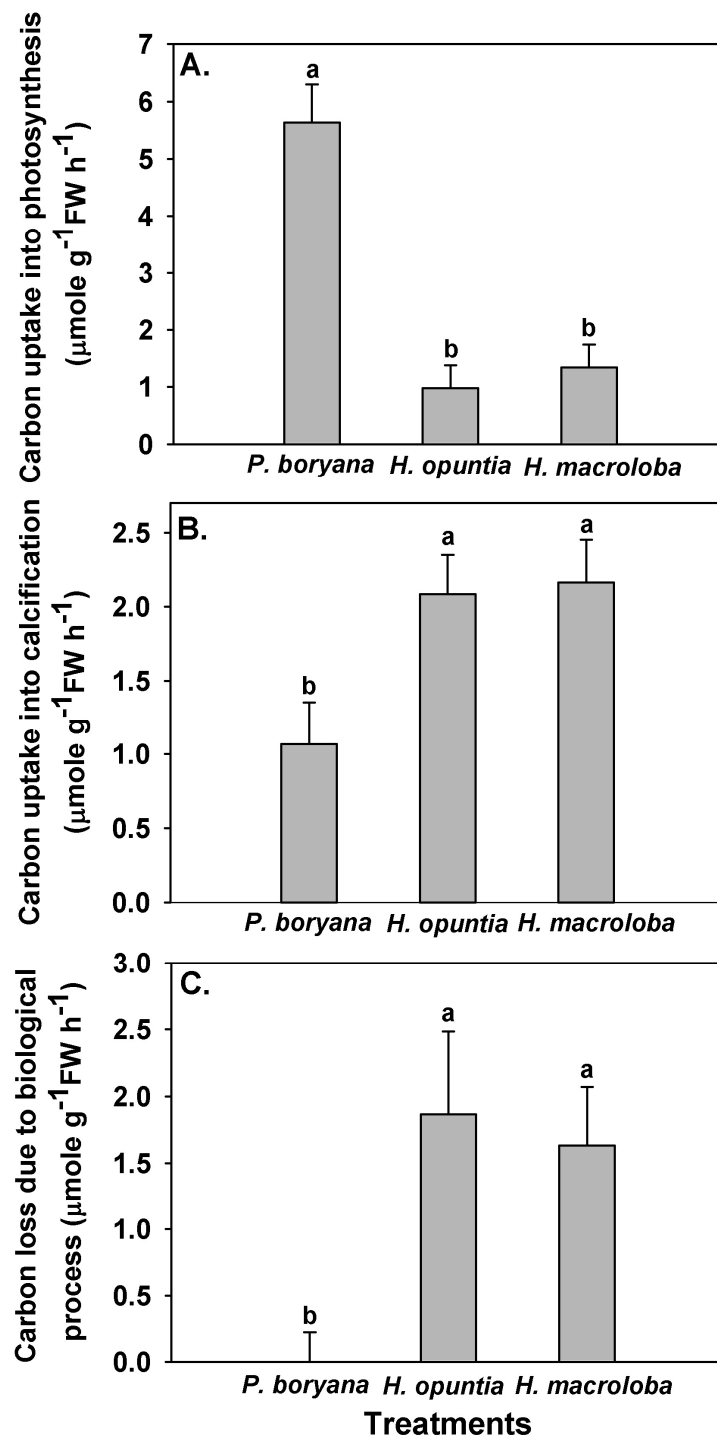
Figure 3. Carbon uptake by photosynthesis (**A**), carbon removal by calcification (**B**) and carbon lost to the air due to incubation (**C**) with *Padina boryana*, *Halimeda opuntia* and *Halimeda macroloba* under an irradiance of 150 μmol photons $m^{-2} s^{-1}$. The fates of carbon were calculated according to Kalokora et al. [20]. Different letters above the bar indicate statistical difference (Fisher's LSD test, $p < 0.05$). Data are means $\pm$ SE (n = 9).

There was a significant positive relationship between carbon removal by calcification and carbon loss to air in *P. boryana* and *H. opuntia* (Figure 4A, $p = 0.005$ in *P. boryana* and $p = 0.0124$ in *H. opuntia*), although both were not significantly related in *H. macroloba* ($p = 0.0658$). A trend line with an intercept = 0 was fitted using all the data points, and the ratio of carbon loss to air to carbon removal by calcification was 0.78. In addition, a

significant positive relationship between photosynthetic carbon uptake and removal by calcification was detected in all species tested (Figure 4B, p = 0.0251, 0.0066 and 0.0223 in *P. boryana*, *H. opuntia* and *H. macroloba*, respectively). Photosynthetic carbon uptake caused 59.44%, 73.441% and 60.90% of the variation in carbon removal by calcification in *P. boryana*, *H. opuntia* and *H. macroloba*, respectively.
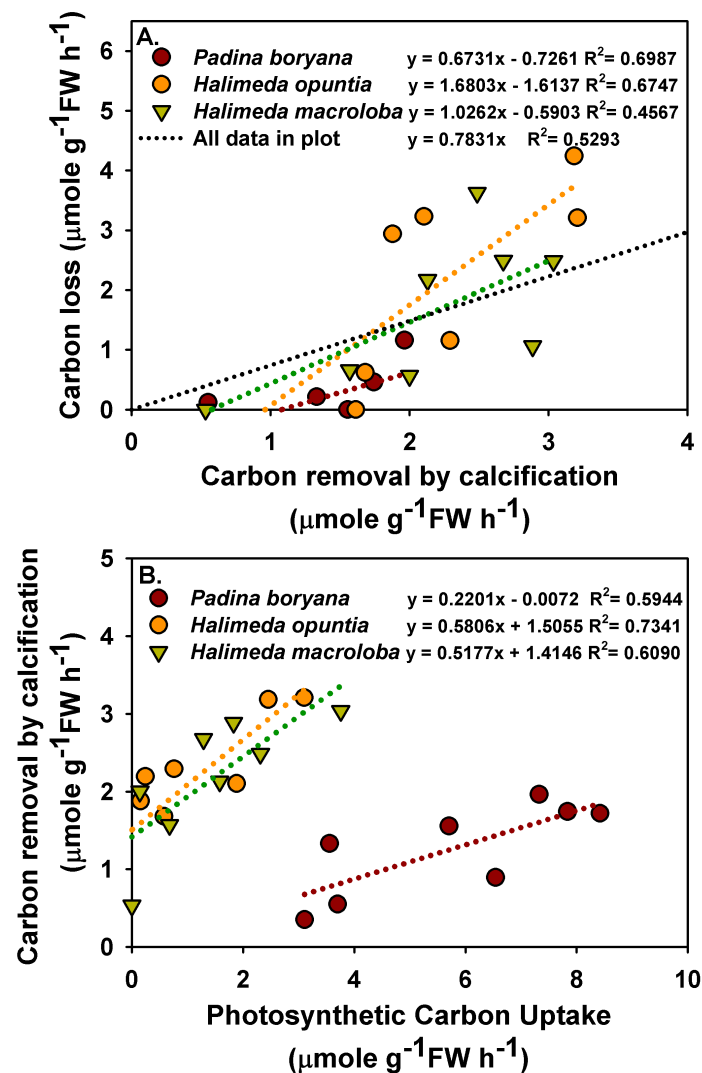

Figure 4. Relationship between carbon removal by calcification and carbon lost to air (**A**) and between photosynthetic carbon uptake and removal by calcification (**B**) in treatments incubated with *Padina boryana*, *Halimeda opuntia* and *Halimeda macroloba*. Fittings using linear regressions are shown as dotted lines, and the equations are displayed. Data are obtained from calculations shown in Figure 3.

Inhibition of light reactions of photosynthesis affected the calcification rates of the three macroalgae and the pH drift of the seawater (Figure 5). Significant effects of incubation conditions (light and darkness) on calcification rates of the three macroalgae were detected (repeated-measures ANOVA, $p < 0.001$, Figure 5A). Similar to the results reported in Figure 3, calcification rates in *P. boryana* were lower than those in *H. opuntia* and *H. macroloba* (Fisher's LSD test, $p < 0.05$). Calcification rates were lowered when macroalgae were incubated in darkness (Fisher's LSD test, $p < 0.05$). *P. boryana* and *H. opuntia* maintained positive net calcification rates in darkness; however, net dissolution was detected in *H. macroloba*. Treatment with DCMU had a strong impact on the calcification process (repeated-measures ANOVA, $p < 0.001$) and induced dissolution in all species tested (Figure 5B). Seawater pH (Figure 5C,D) was affected by macroalgal species (repeated-measures ANOVA, $p < 0.001$), incubation conditions (repeated-measures ANOVA, $p < 0.001$) and interaction

of the two factors (repeated-measures ANOVA, $p < 0.001$). Incubation conditions did not result in significant change in seawater pH of controls, indicating that changes observed in other treatments were associated with biological processes. An increase in seawater pH was detected after *P. boryana* was exposed to light for 1 h (Fisher's LSD test, $p < 0.05$), whereas seawater from the incubation with *H. opuntia* and *H. macroloba* remained comparable to controls. Incubation in darkness resulted in a lower seawater pH as compared to incubation in the light in all treatments containing macroalgae (Fisher's LSD test, $p < 0.05$, Figure 5C). Similar results were observed in the presence of DCMU (Figure 5D).
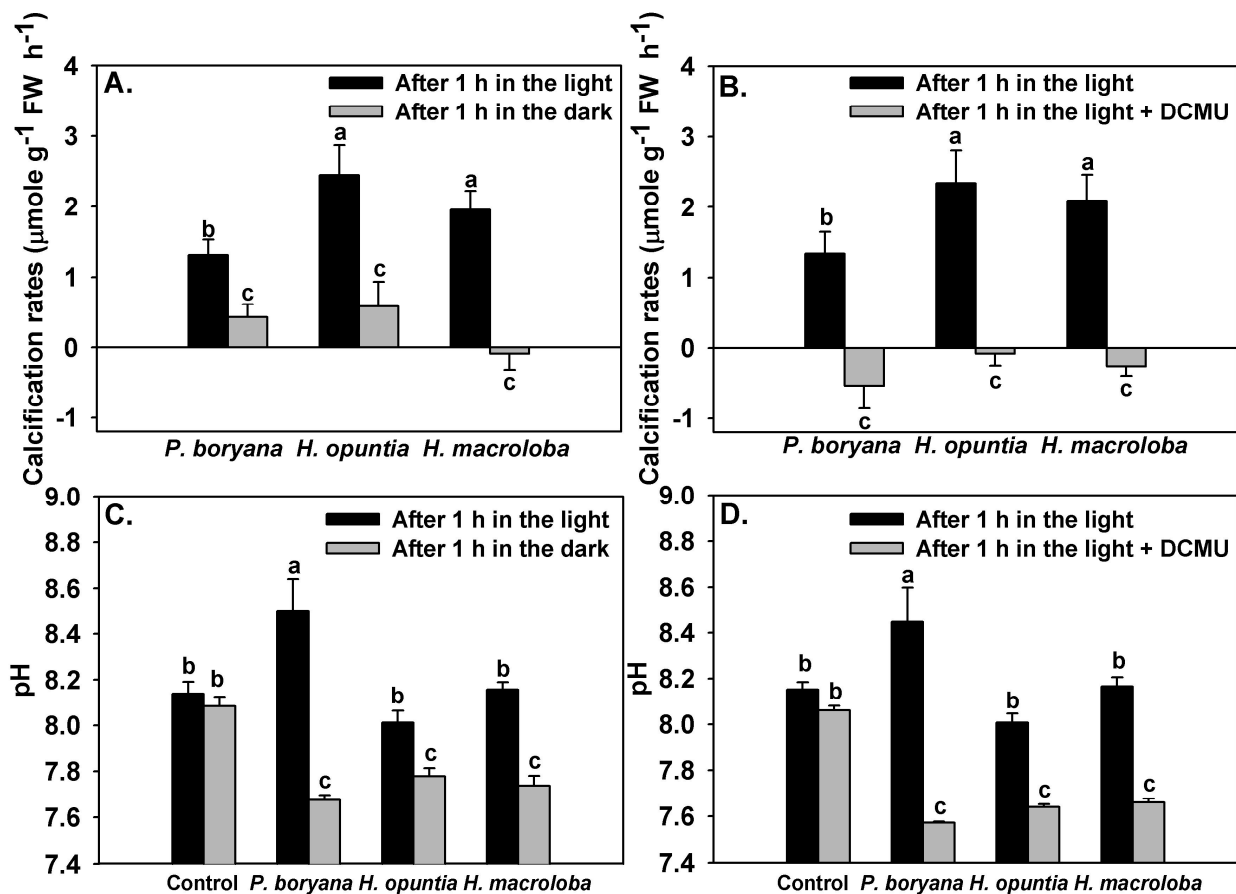

Figure 5. Effects of inhibition of photosynthesis on calcification rates of *Padina boryana*, *Halimeda opuntia* and *Halimeda macroloba* (**A,B**) and seawater pH (**C,D**) after 1 h incubation under an irradiance of 150 µmol photons m^{-2} s^{-1}. Bars without shared letters are considered statistically different (Fisher's LSD test, $p < 0.05$). Data are means $\pm$ SE (n = 9).

3. Discussion

Our study showed that the biological processes of *P. boryana*, *H. opuntia* and *H. macroloba* significantly alter seawater chemistry but to a different extent, which is probably due to differences in photosynthetic carbon uptake and calcification. While both photosynthetic carbon fixation and calcification contributed to total DIC uptake in *P. boryana*, photosynthesis appears to be the main driver for a drastic decrease in DIC and a rise in seawater pH. In contrast, DIC uptake of *H. opuntia* and *H. macroloba* were largely associated with calcification and to a lesser extent, with photosynthesis, resulting in a change in pH with smaller magnitude. Higher calcification rates in *H. opuntia* and *H. macroloba* compared to *P. boryana* may also explain their higher accumulation of CaCO$_3$ (1.6–1.7 times higher than in *P. boryana*).

Both *Padina* and *Halimeda* were identified as active HCO$_3^-$ and CO$_2$ users by means of CCMs [48]. Both can readily utilize HCO$_3^-$ for photosynthesis, although their actual mechanisms may differ depending on their modes of calcification [48,49]. Morphological characteristics and site of calcification influence calcification and photosynthetic pro-

cess [39,50,51]. The sheet-like thallus of *P. boryana* has higher specific surface area than *H. opuntia* and *H. macroloba* thus they are expected to exhibit higher productivity and more efficient nutrient uptake for the same weight [52]. The morphology of primary utricle in *Halimeda* (e.g., size, orientation) and their lateral adhesion between adjacent primary utricles likely affect the diffusion pathway and ions uptake for $CaCO_3$ precipitation (e.g., Ca^{2-}, CO_3^{2-}) [39,50,51]. Diffusion pathways between primary utricles also control H^+ fluxes from the bulk seawater into the primary interutricle spaces or removal of H^+, a product of calcification, from the primary interutricle spaces to prevent H^+ accumulation [39]. In addition, shorter diffusion pathway may lead to lower diffusive resistance for the influx of Ca^{2+} and potentially HCO_3^- or CO_3^{2-} from seawater to primary interutricle space, which potentially increases $CaCO_3$ precipitation [39,50]. This suggests lower energetic cost to *H. opuntia* than *H. macroloba* in calcification [53–55], which might explain the higher $CaCO_3$ content with larger crystal length and width and smaller crystal density in *H. opuntia* with a smaller surface diameter of the primary utricle and lower diffusion pathway length than *H. macroloba*. Our findings were also consistent with Peach et al. [39], which found strong inverse relationship between average $CaCO_3$ content and primary utricle surface diameter.

Variability in calcification rates in relation to photosynthesis among the three macroalgae corresponded well with reduced total alkalinity which did not recover after equilibration. In *H. opuntia* and *H. macroloba*, TA and DIC were decreased after incubation and remained low after equilibration, implying that CO_2 loss from the seawater took place, which was consistent with a recent study in *Corallina officinalis* [20]. In contrast, with lightly calcified algae, *P. boryana* was more engaged in photosynthetic carbon uptake than in calcification, thus resulting in no net carbon loss. In this study, a positive correlation between carbon loss to air and calcification was presented, and the ratio of carbon loss to air to carbon removal by calcification was 0.78. This estimate is comparable to the values reported in *C. officinalis* (0.78; [20]) and slightly higher than those reported in the coral reefs (0.6; [56]). Notably, when each species was analyzed separately, different functional constants were obtained. These constants suggest that in order to obtain net carbon loss, a certain rate of calcification must be reached (negative y-intercept). While the results generally imply that macroalgal calcification may act as a source of CO_2, the carbon economy of the coastal community is controlled by multiple processes. Kalokora et al. [20] suggested that the released CO_2 may be refixed by a photosynthetic process, particularly of marine primary producers, such as seagrasses and other macrophytes. In Thai waters and other tropical habitats, calcified macroalgae, especially species from genus *Halimeda*, were often found coexisting with fleshy macroalgae and seagrasses [57–59]. Therefore, community photosynthesis may enhance calcification by increasing the pH and saturation state of $CaCO_3$ in the surrounding seawater and simultaneously capture CO_2 released from calcification during daytime [12,57].

There was a significant positive relationship between photosynthetic carbon uptake and carbon removal by calcification in all species tested, similar to previous studies in other calcifying algae [20,28,60–62]. Our findings provide supporting evidence that calcification and photosynthesis in *P. boryana*, *H. opuntia* and *H. macroloba* are closely coupled [24,28,32,63,64] but contradict the results of a study on the congeneric species, *Padina pavonica* and *Padina japonica*, which reported a lack of correlation between photosynthesis and carbonate deposition [40]. These discrepant results may be due to differences in calcification capacity, which was significantly higher in *P. boryana* in the present study [40]. This coupling between photosynthesis and calcification is mediated by a localized modification of seawater chemistry, generating a suitable microenvironment for photosynthesis and calcification. Calcium carbonate deposition of an individual promotes photosynthesis via an increase in proton extrusion, which subsequently increases CO_2 availability readily for photosynthetic carbon uptake of the same individual [20,25,32,65]. Meanwhile, photosynthesis elevates the pH and saturation state of $CaCO_3$ at the macroalgal thalli surface diffusive boundary layer and at the calcification site, thus promoting calcification [25,31,42,66,67]. Beer and Larkum [64] suggested that calcification in *Halimeda discoidea* is linked to pH

in intercellular spaces controlled by the ratio of photosynthesis to respiration. Recent studies have revealed that higher pH at the diffusive boundary layer in the light in many tropical calcified macroalgae, including *Halimeda*, is maintained by photosynthetic CCM involving a HCO_3^-–H^+ symport, OH^- antiport and HCO_3^- dehydration catalyzed by external carbonic anhydrase [14,28]. Our study showed that approximately 4.5–4.7 mols of carbon were taken in photosynthesis for every mol carbon fixed into calcification in *P. boryana*. While regressions in *H. opuntia* and *H. macroloba* did not show the x and y intercepts of zero, approximately 0.5–1.0 and 0.5–1.2 mols of carbon were taken in photosynthesis for every mol carbon fixed into calcification in *H. opuntia* and *H. macroloba*, respectively. Different ratio numbers were reported in previous studies: 4–8 for *Halimeda* [68], 1.6 for four deep-water *Halimeda* [63] and 1 and 1.5 for *C. officinalis*, respectively [20,60], indicating that this is a variable depending on local adaptation and not only species-specific.

The dependency of calcification on photosynthesis was further illustrated in the subsequent experiment in which both light-dependent and photosystem II (PSII) electron transport-dependent calcification was observed. Incubation in darkness significantly reduced calcification rates in all tested species and simultaneously reduced seawater pH. As *H. opuntia* and *H. macroloba* deposit aragonite crystals in the intercellular space between utricles, which is semi-separated from external seawater, these algae may be more resistant to the pH change in surrounding water than *P. boryana*, which precipitate aragonite crystals externally at the thallus surface [40,68,69]. However, our results indicate that *P. boryana* was the least pH-sensitive, sustaining the highest percentage of calcification rate relative to the rates in the light (approx. 33%) at the lowest final pH (7.67 ± 0.02). This is evident as *Padina* is among the persistent macroalgal genus in acidified environments [38,41,70–74]. Meanwhile, *H. macroloba* was the most sensitive species, displaying net dissolution after 1 h of darkness at the highest pH (7.74 ± 0.04) among all species. Minimal calcification and dissolution were also observed in species from genus *Halimeda* in the field condition at nighttime [13,14,75]. Differences in sensitivity to pH between *H. opuntia* and *H. macroloba* may be due to different morphological characteristics, such as branching and crystal microstructure [76]. While multitudinous branches forming tight complex structures in *H. opuntia* may generate greater diffusive boundary layer thickness and consequently allowing better regulation of their microenvironment as previously observed in coralline algae [77], shorter and thinner crystals found in *H. macroloba* may be more susceptible to dissolution and may require more crystal nucleation, which is a major rate-limiting step for precipitation of $CaCO_3$ [78]. In addition, inhibiting PSII electron transport using DCMU imposed stronger negative effects on calcification of all tested species, with *P. boryana* as the most affected. This emphasizes that certain mechanisms associated with calcification are species specific, and the processes and factors associated with functioning photosynthetic electron transport are more important facilitators of calcification than other light-dependent but PSII-independent processes, such as light-triggered H^+ transport pumps [28,31,64]. Nevertheless, more adverse effects of DCMU could be attributed to a lower pH in the seawater, promoting dissolution in all species [13,38]. Comparisons among different species of calcified macroalgae in our study suggest that $CaCO_3$ precipitation is linked to photosynthesis and pH, and may vary depending on the morphological features. However, these interrelations remain unclear and require further investigations.

Our results provide experimental evidence that calcification of the three common calcified macroalgae in Phuket, Thailand is a potential source of CO_2, supporting a recent study on *C. officinalis* [20]. Calcification by *H. opuntia* and *H. macroloba* lead to greater loss in CO_2 per biomass weight than *P. boryana*. Nevertheless, this capacity varies on a diurnal basis, as calcification is highly coupled to photosynthetic activity. Our results also imply that future acidification will impose more negative effects on *H. opuntia* and *H. macroloba* than on *Padina boryana*, and the effects on calcified macroalgae may be worsened in darkness. Therefore, further investigations on the carbon budget of the coastal ecosystem should account for calcification as a potential carbon source while considering diurnal

variations and the buffering capacity of the primary production of marine vegetation in the natural setting [12,26,57].

4. Materials and Methods

4.1. Sampling and Acclimatization

P. boryana, *H. opuntia* and *H. macroloba* were carefully collected with their holdfasts intact from Tung Khen Bay, Phuket (7.810057; 98.404100), where all species were found in high densities and growing on calcareous sediment with depth between 0.5 and 1.0 m. As our investigations were solely focused on the populations growing in the upper sublittoral areas, differences due to varying depth and irradiance were not considered. Cleaned samples were transported to the aquaria facility of Coastal Oceanography and Climate Change Research Center, Prince of Songkla University, in cool boxes containing seawater collected from the sampling site. Additional seawater was collected in sealed dark polypropylene bottles and fixed when necessary. Seawater pH, salinity and total alkalinity (TA) were immediately determined upon arrival at the laboratory (pH = 8.1, salinity = 30 and TA = 2.04 ± 0.05 mM).

At our aquaria facility, the samples were rinsed to remove the remaining sediment and epiphytes. Collected samples were maintained in aquaria filled with sterile seawater (pH = 8.1, salinity = 30 PSU and TA = 1.90 ± 0.08 mM) with constant aeration under ambient temperature (27 °C–32 °C). The irradiance of approximately 150 μmol photons $m^{-2} s^{-1}$ was provided with aquarium LED light (A601, Chihiros, Cixi, Zhejiang, China) with a 12:12 h light–dark cycle. An irradiance of 150 μmol photons $m^{-2} s^{-1}$ (measured using LI-250A light meter; LICOR, Germany) was chosen based on the minimal saturating irradiance (E_k) derived from the rapid light curves (RLC; Ralph and Gademann [79]) conducted using the collected samples (data not shown). Throughout the acclimation period, pH, salinity and TA were monitored regularly to avoid changes due to evaporation, and distilled water was added as necessary. Prior to the experiment, the health of the macroalgae was evaluated by a pulse amplitude modulated fluorometer (Diving-PAM, Walz, Effeltrich, Germany) using the maximum quantum yield (F_v/F_m) as a biomarker. Subsequent experiments were carried out with algal thalli with an $F_v/F_m \geq 0.7$. Experiments were conducted within 7 days of the collection date after which the samples were discarded and fresh materials were collected. Each experimental run consists of all species and all treatments. The run was repeated with new biological materials.

4.2. Characterization of Calcification and Its Effect on Seawater Chemistry

4.2.1. Experimental Design

Each macroalga was weighed to reach the wet weight of approximately 5 g and placed in 250 mL flasks containing a magnetic bar (0.4 × 1.0 cm in size) and filled with 250 mL of seawater. The flasks were tightly closed with rubber stoppers and securely wrapped with parafilm. Flasks filled with seawater without macroalgae were used as controls and were included in the experiment. The flasks were arranged on top of magnetic stirrers where mixing occurs and the effect of the diffusive boundary layer was minimized. The assembly of the experimental set-up was done in dimmed light. Subsequently, an irradiance of approximately 150 μmol photons $m^{-2} s^{-1}$ was provided by aquarium LED light (A601, Chihiros, China) for 3 h. The light source was positioned on the side so that the macroalgae were not shaded by the stoppers. When incubation in the light was finished, the macroalgae were removed from the flasks. The remaining seawater without macroalgae was then allowed to be equilibrated with air using a compressed air pump for an additional 4 h (the minimum duration for the seawater to reach stable pH, predetermined from the preliminary results). The macroalgae from each flask were rinsed and dried using a paper towel and kept at −20 °C for further assessment of the surface area, $CaCO_3$ accumulation and microstructural analyses (See below).

Parameters related to seawater chemistry, namely seawater pH, TA and salinity, were measured at three steps: (1) the initial step before light exposure, (2) after 3 h of light

exposure and (3) after equilibration with air. Seawater temperature was also recorded. These parameters were used to calculate total dissolved inorganic carbon (DIC), calcification rates, photosynthetic carbon uptake and carbon loss to air, further detailed in Section 4.2.3. Measurements for each species and each treatment were based on nine biological replicates (n = 9).

4.2.2. Determination of Surface Area, CaCO$_3$ Accumulation and Microstructural Analyses

Thalli of *P. boryana*, *H. macroloba* and *H. opuntia* were cut into parts (individual lobe for *P. boryana* and individual segment for *H. macroloba* and *H. opuntia*) and spread on a surface lined with rulers, and the image of each sample was taken. The surface area was determined using image processing software (ImageJ V. 1.53e, Rasband W.S., U.S. National Institute of Health, Bethesda, Maryland, USA) from images of samples [80,81].

Samples were rinsed with distilled water and dried until constant weight at 60 °C. The CaCO$_3$ accumulation of each sample was investigated by dissolving thalli in 5% HCl for 1 h and measuring the dry weights before and after CaCO$_3$ dissolution using an electronic balance [27].

Images of aragonite CaCO$_3$ crystals were examined using a scanning electron microscope (SEM Apreo, FEI, Czech Republic) at the Office of Scientific Instrument and Testing, Prince of Songkla University. The instrument was operated at 20 kV w in high vacuum mode and imaged using the secondary in-lens detector. Samples were mounted on aluminum stubs and then placed in a gold coating unit (SPI Supplies, USA) operated at a 40 mm working distance. Length, width and density of aragonite crystals (n = 4–6) were determined using image processing software. Aragonite crystals with complete needle structure at the top layer in the images were chosen. Ten crystals per replicate were used to calculate average size following the method described by Sinutok et al. [35].

Thalli of *P. boryana* and apical segments of *Halimeda* were fixed in 2% glutaraldehyde in 0.05 M phosphate buffered saline and stored at 4 °C. Fixed samples were posted-fixed in 1% OsO4 buffer, and dehydrated through a series of ethanol concentrations (70%, 80%, 90% and 100%). Samples embedded in epoxy resin and were cut into thin sections (80 nm) using a microtome (MT XL microtome, RMC, USA) and stained with 2% uranyl acetate (3 min). Stained sections of *P. boryana* were examined with a transmission electron microscope at 160 kV (JOEL, JEM-2010, Japan), while stained sections of *H. opuntia* and *H. macroloba* were examined using a compound microscope (DM500, Leica Microsystems, Germany). Surface diameter of primary utricle (pU) and diffusion pathway length were determined using image processing software as previously described.

4.2.3. Determination of Carbonate Chemistry-Related Parameters and Fates of Carbon Related to Biological Processes

To avoid creating large headspace in incubation flasks, parameters related to seawater chemistry at the initial step were determined from the samplings drawn from the prepared seawater for the experiment and not directly from the flasks. After light exposure and after equilibration, seawater was collected from each flask using a 50 mL syringe with an extended rubber tube. Total alkalinity was determined using a total alkalinity mini-titrator for water analysis (HI-84531-02, Hanna Instruments, Woonsocket, RI, USA) according to the manufacturer's instruction. Salinity was measured using an optical refractometer, and seawater pH was measured using a bench-top pH meter (Ohaus RL150, Russell, USA) according to the manufacturer's instructions.

The measured seawater chemistry parameters were later used to calculate DIC, its distribution among different forms (CO_2, HCO_3^- and CO_3^{2-}) and saturation state of aragonite (ΩAr) and calcite (ΩCa). Calculation was performed using the software CO_2 sys.xls [82].

Calcification rates were calculated following alkalinity anomaly protocol (as described in [20]), whereby a decrease in TA by two equivalents when one mole of CaCO$_3$ is precipitated [83,84]. Calcification rates were normalized against macroalgal wet weight.

In addition to calcification rates, the difference in DIC and TA in seawater collected at the initial time point after incubation in the light and after equilibration can estimate photosynthetic carbon uptake and carbon loss from the seawater surrounding the macroalga. Estimation of photosynthetic carbon uptake and carbon loss was done as described by Kalokora et al. [20] using the following equations:

$$\text{Photosynthetic carbon uptake} = (\text{DIC}_{\text{initial}} - \text{DIC}_{\text{after light incubation}}) - \text{DIC}_{\text{calcification}} \quad (1)$$

$$\text{Carbon loss} = (\text{DIC}_{\text{initial}} - \text{DIC}_{\text{after equilibration}}) - \text{DIC}_{\text{calcification}} \quad (2)$$

4.3. Interrelation between Photosynthesis and Calcification

Downscaled and shortened setups were adopted for this experiment. Each macroalga with known and similar wet weight (5 g) was placed in 125 mL flasks filled with 140 mL of sterilized seawater. Measurements for each species and each treatment were based on five biological replicates (n = 5).

This experiment was designed to compare calcification rates in the light to those obtained when photosynthetic light reactions were inhibited. First, we compared calcification rates in light and darkness. During the light exposure, an irradiance of approximately 150 µmol photons m^{-2} s^{-1} was provided for 1 h (Aquarium LED light A601, Chihiros, China). Calcification rates in the light were calculated from the TA measured before and after light exposure as previously described. The seawater was subsequently replaced, and macroalgae were maintained in fresh seawater in darkness for an additional 1 h. Calcification rates in the dark (Calcification$_{\text{dark}}$) were calculated from the TA measured before and after incubation in darkness. Flasks filled with seawater without macroalgae were used as negative controls. Second, we compared calcification rates in the light and in the presence of 0.1 mM 3(3,4-dichlorophenyl)-1,1-dimethylurea (DCMU, the concentration was selected based on the preliminary test, data not shown). Calcification rates in the light were calculated from the TA measured before and after 1 h of light exposure as previously described. The seawater was subsequently replaced with seawater containing 0.5 mM DCMU, and irradiance was provided for an additional 1 h. DCMU inhibits photosynthetic electron transport from PSII to plastoquinone and is widely used as an inhibitor of photosynthesis [85]. The use of DCMU can determine whether the calcification and photosynthetic electron transport are interrelated [64,86]. Seawater prepared for the measurements of calcification rates in the light contained the same volume of ethanol used as the solvent in DCMU treatment (70 µL, corresponding to 0.05% *v/v*). Flasks filled with seawater without macroalgae were used as negative controls. Calcification rates in the presence of DCMU (Calcification$_{\text{dcmu}}$) were calculated from the TA measured before and after incubation in the light. Seawater pH at the end of each step was also recorded.

4.4. Statistical Analyses

All the analyses were performed using Statistica academic platform version 13.0 (StatSoft, Tulsa, OK, USA). Cochran's test was used to verify the assumption of homogeneity of variance prior to conducting the analysis of variance (ANOVA). The statistical significance level was set at $p < 0.05$ in all analyses.

Differences in %CaCO$_3$ and the CaCO$_3$ crystal morphology and densities among species were analyzed using one-way ANOVA. The difference in surface diameter of primary utricles (pU) diffusion pathway length was analyzed using a *t*-test.

To characterize the effects of calcification and its effect on seawater chemistry, water chemistry and calcification rates were analyzed by repeated-measures ANOVA using the time of measurements as the within-group factor and macroalgal species as the categorical factor. Differences in each fate of carbon (carbon uptake by photosynthesis, carbon removal by calcification and carbon lost to the air) among species were analyzed using one-way ANOVA. Fisher's least significant difference (LSD) test was used to compare these parameters across treatments. The relationships between calcification and carbon loss and between photosynthesis and calcification were analyzed by linear regression.

Effects of inhibition of photosynthesis on seawater pH and calcification rates were tested by repeated-measures ANOVA using time of measurements as the within-group factor and macroalgal species as the categorical factor. Fisher's LSD test was used to compare these parameters across treatments.

References

1. Houghton, J.T.; Ding, Y.; Griggs, D.J.; Noguer, M.; van der Linden, P.J.; Dai, X.; Maskell, K.; Johnson, C.A. *Climate Change 2001: The Scientific Basis. Contribution of Working Group I to the Third Assessment Report of the Intergovernmental Panel on Climate Change*; Cambridge University Press: Cambridge, UK, 2001.
2. Meehl, G.A.; Stocker, T.F.; Collins, W.D.; Friedlingstein, P.; Gaye, A.T.; Gregory, J.M.; Kitoh, A.; Knutti, R.; Murphy, J.M.; Noda, A.; et al. Global Climate Projections. In *Climate Change 2007: The Physical Science Basis. Contribution of Working Group I to the Fourth Assessment Report of the Intergovernmental Panel on Climate Change*; Cambridge University Press: Cambridge, NY, USA, 2007.
3. Albright, R.; Benthuysen, J.; Cantin, N.; Caldeira, K.; Anthony, K. Coral reef metabolism and carbon chemistry dynamics of a coral reef flat. *Geophys. Res. Lett.* **2015**, *42*. [CrossRef]
4. Rasmusson, L.M.; Nualla-ong, A.; Wutiruk, T.; Björk, M.; Gullström, M.; Buapet, P. Sensitivity of photosynthesis to warming in two similar species of the aquatic angiosperm *Ruppia* from tropical and temperate habitats. *Sustainability* **2021**, *13*, 9433. [CrossRef]
5. Yucharoen, M.; Sinutok, S.; Chotikarn, P.; Buapet, P. Experimental assessment of vulnerability to warming in tropical shallow-water marine organisms. *Front. Mar. Sci.* **2021**, *8*, 767628. [CrossRef]
6. Tano, S.; Eggertsen, M.; Wikström, S.A.; Berkström, C.; Buriyo, A.S.; Halling, C. Tropical seaweed beds are important habitats for mobile invertebrate epifauna. *Estuar. Coast. Shelf Sci.* **2016**, *183*, 1–12. [CrossRef]
7. Eggertsen, L.; Ferreira, C.E.L.; Fontoura, L.; Kautsky, N.; Gullström, M.; Berkström, C. Seaweed beds support more juvenile reef fish than seagrass beds in a south-western Atlantic tropical seascape. *Estuar. Coast. Shelf Sci.* **2017**, *196*, 97–108. [CrossRef]
8. Hill, R.; Bellgrove, A.; Macreadie, P.I.; Petrou, K.; Beardall, J.; Steven, A.; Ralph, P.J. Can macroalgae contribute to blue carbon? An Australian perspective. *Limnol. Oceanogr.* **2015**, *60*, 1689–1706. [CrossRef]
9. Krause-Jensen, D.; Lavery, P.; Serrano, O.; Marbà, N.; Masque, P.; Duarte, C.M. Sequestration of macroalgal carbon: The elephant in the Blue Carbon room. *Biol. Lett.* **2018**, *14*, 20180236. [CrossRef]
10. Raven, J. Blue carbon: Past, present and future, with emphasis on macroalgae. *Biol. Lett.* **2018**, *14*, 20180336. [CrossRef]
11. Ortega, C.; Vargas, G.; Rojas, M.; Rutllant, J.A.; Muñoz, P.; Lange, C.B.; Pantoja, S.; Dezileau, L.; Ortlieb, L. Extreme ENSO-driven torrential rainfalls at the southern edge of the Atacama Desert during the Late Holocene and their projection into the 21th century. *Glob. Planet. Chang.* **2019**, *175*, 226–237. [CrossRef]
12. Bergstrom, E.; Silva, J.; Martins, C.; Horta, P. Seagrass can mitigate negative ocean acidification effects on calcifying algae. *Sci. Rep.* **2019**, *9*, 1932. [CrossRef] [PubMed]
13. McNicholl, C.; Koch, M.S.; Swarzenski, P.W.; Oberhaensli, F.R.; Taylor, A.; Batista, M.G.; Metian, M. Ocean acidification effects on calcification and dissolution in tropical reef macroalgae. *Coral Reefs* **2020**, *39*, 1635–1647. [CrossRef]
14. McNicholl, C.; Koch, M.S. Irradiance, photosynthesis and elevated pCO$_2$ effects on net calcification in tropical reef macroalgae. *J. Exp. Mar. Bio. Ecol.* **2021**, *535*, 151489. [CrossRef]
15. Yang, F.; Wei, Z.; Long, L. Transcriptomic and Physiological Responses of the Tropical Reef Calcified Macroalga *Amphiroa fragilissima* to Elevated Temperature[1]. *J. Phycol.* **2021**, *57*, 1254–1265. [CrossRef]

16. Johnson, M.D.; Price, N.N.; Smith, J.E. Contrasting effects of ocean acidification on tropical fleshy and calcareous algae. *PeerJ* **2014**, *2*, e411. [CrossRef]

17. Arina, N.; Raynusha, C.; Hidayah, N.; Zainee, N.F.A.; Prathep, A.; Rozaimi, M. Coralline macroalgae contribution to ecological services of carbon storage in a disturbed seagrass meadow. *Mar. Environ. Res.* **2020**, *162*, 105156. [CrossRef]

18. Kleypas, J.A.; Anthony, K.R.N.; Gattuso, J.-P. Coral reefs modify their seawater carbon chemistry—Case study from a barrier reef (Moorea, French Polynesia). *Glob. Chang. Biol.* **2011**, *17*, 3667–3678. [CrossRef]

19. Macreadie, P.I.; Anton, A.; Raven, J.A.; Beaumont, N.; Connolly, R.M.; Friess, D.A.; Kelleway, J.J.; Kennedy, H.; Kuwae, T.; Lavery, P.S.; et al. The future of Blue Carbon science. *Nat. Commun.* **2019**, *10*, 3998. [CrossRef] [PubMed]

20. Kalokora, O.J.; Buriyo, A.S.; Asplund, M.E.; Gullström, M.; Mtolera, M.S.P.; Björk, M. An experimental assessment of algal calcification as a potential source of atmospheric CO_2. *PLoS ONE* **2020**, *15*, e0231971. [CrossRef]

21. Ware, J.R.; Smith, S.V.; Reaka-Kudla, M.L. Coral reefs: Sources or sinks of atmospheric CO_2? *Coral Reefs* **1992**, *11*, 127–130. [CrossRef]

22. Frankignoulle, M.; Canon, C.; Gattuso, J.-P. Marine calcification as a source of carbon dioxide: Positive feedback of increasing atmospheric CO_2. *Limnol. Oceanogr.* **1994**, *39*, 458–462. [CrossRef]

23. Barker, S.; Higgins, J.A.; Elderfield, H. The future of the carbon cycle: Review, calcification response, ballast and feedback on atmospheric CO_2. *Philos. Trans. R. Soc. London. Ser. A Math. Phys. Eng. Sci.* **2003**, *361*, 1977–1999. [CrossRef]

24. Borowitzka, M.A. Calcification in aquatic plants. *Plant Cell Environ.* **1984**, *7*, 457–466. [CrossRef]

25. McConnaughey, T. Biomineralization Mechanisms. In *Origin, Evolution, and Modern Aspects of Biomineralization in Plants and Animals*; Springer: Bostan, MA, USA, 1989.

26. Buapet, P.; Gullström, M.; Björk, M. Photosynthetic activity of seagrasses and macroalgae in temperate shallow waters can alter seawater pH and total inorganic carbon content at the scale of a coastal embayment. *Mar. Freshw. Res.* **2013**, *64*, 1040–1048. [CrossRef]

27. Sinutok, S. Interactive Effects of the Ocean Acidification and Warming on Sediment Dwelling Marine Calcifers. Ph.D. Thesis, University of Technology Sydney, Sydney, Australia, 2013.

28. McNicholl, C.; Koch, M.S.; Hofmann, L.C. Photosynthesis and light-dependent proton pumps increase boundary layer pH in tropical macroalgae: A proposed mechanism to sustain calcification under ocean acidification. *J. Exp. Mar. Bio. Ecol.* **2019**, *521*, 151208. [CrossRef]

29. Van der Heijden, L.H.; Kamenos, N.A. Calculating the global contribution of coralline algae to carbon burial. *Biogeosciences* **2015**, *12*, 7845–7877. [CrossRef]

30. Hofmann, L.C.; Bischof, K.; Baggini, C.; Johnson, A.; Koop-Jakobsen, K.; Teichberg, M. CO_2 and inorganic nutrient enrichment affect the performance of a calcifying green alga and its noncalcifying epiphyte. *Oecologia* **2015**, *177*, 1157–1169. [CrossRef]

31. Hofmann, L.C.; Koch, M.; de Beer, D. Biotic control of surface pH and evidence of light-induced H^+ pumping and Ca^{2+}-H^+ exchange in a tropical crustose coralline alga. *PLoS ONE* **2016**, *11*, e0159057. [CrossRef]

32. Sinutok, S.; Hill, R.; Doblin, M.A.; Kühl, M.; Ralph, P.J. Microenvironmental changes support evidence of photosynthesis and calcification inhibition in *Halimeda* under ocean acidification and warming. *Coral Reefs* **2012**, *31*, 1201–1213. [CrossRef]

33. Schulz, K.G.; Riebesell, U. Diurnal changes in seawater carbonate chemistry speciation at increasing atmospheric carbon dioxide. *Mar. Biol.* **2013**, *160*, 1889–1899. [CrossRef] [PubMed]

34. Sinutok, S.; Pongparadon, S.; Prathep, A. Seasonal variation in density, growth rate and calcium carbonate accumulation of *Halimeda macroloba* Decaisne at Tangkhen Bay, Phuket Province, Thailand. *Malays. J. Sci.* **2008**, *27*, 1–8.

35. Sinutok, S.; Hill, R.; Doblin, M.A.; Wuhrer, R.; Ralph, P.J. Warmer more acidic conditions cause decreased productivity and calcification in subtropical coral reef sediment-dwelling calcifiers. *Limnol. Oceanogr.* **2011**, *56*, 1200–1212. [CrossRef]

36. Kleypas, J.A.; Buddemeier, R.W.; Archer, D.; Gattuso, J.-P.; Langdon, D.; Opdyke, B.N. Geochemical consequences of increased atmospheric carbon dioxide on coral reefs. *Science* **1999**, *284*, 118–120. [CrossRef] [PubMed]

37. Hofmann, L.C.; Bischof, K. Ocean acidification effects on calcifying macroalgae. *Aquat. Biol.* **2014**, *22*, 261–279. [CrossRef]

38. Iluz, D.; Fermani, S.; Ramot, M.; Reggi, M.; Caroselli, E.; Prada, F.; Dubinsky, Z.; Goffredo, S.; Falini, G. Calcifying response and recovery potential of the brown alga *Padina pavonica* under ocean acidification. *ACS Earth Sp. Chem.* **2017**, *1*, 316–323. [CrossRef]

39. Peach, K.E.; Koch, M.S.; Blackwelder, P.L.; Manfrino, C. Calcification and photophysiology responses to elevated pCO_2 in six *Halimeda* species from contrasting irradiance environments on Little Cayman Island reefs. *J. Exp. Mar. Bio. Ecol.* **2017**, *486*, 114–126. [CrossRef]

40. Okazaki, M.; Pentecost, A.; Tanaka, Y.; Miyata, M. A study of calcium carbonate deposition in the genus *Padina* (Phaeophyceae, Dictyotales). *Br. Phycol. J.* **1986**, *21*, 217–224. [CrossRef]

41. Johnson, V.R.; Russell, B.D.; Fabricius, K.E.; Brownlee, C.; Hall-Spencer, J.M. Temperate and tropical brown macroalgae thrive, despite decalcification, along natural CO_2 gradients. *Glob. Chang. Biol.* **2012**, *18*, 2792–2803. [CrossRef]

42. Koch, M.; Bowes, G.; Ross, C.; Zhang, X.-H. Climate change and ocean acidification effects on seagrasses and marine macroalgae. *Glob. Chang. Biol.* **2013**, *19*, 103–132. [CrossRef]

43. Wei, Z.; Long, C.; Zhang, Y.; Huo, Y.; Yang, F.; Long, L. Increased light availability enhances tolerance against ocean acidification stress in *Halimeda opuntia*. *bioRxiv* **2020**, *1*, 1–38.

44. Mayakun, J.; Bunruk, P.; Kongsaeng, R. Growth rate and calcium carbonate accumulation of Halimeda macroloba Decaisne (Chlorophyta: Halimedaceae) in Thai waters. *Songklanakarin J. Sci. Technol.* **2014**, *36*, 419–423.

45. Wichachucherd, B.; Prathep, A.; Zuccarello, G.C. Phylogeography of *Padina boryana* (Dictyotales, Phaeophyceae) around the Thai-Malay Peninsula. *Eur. J. Phycol.* **2014**, *49*, 313–323. [CrossRef]

46. Kaewsrikhaw, R.; Prathep, A.; Darakrai, A.; Beer, S. Photosynthesis and calcification in two *Halimeda* species from Phuket, Thailand. *Bot. Mar.* **2016**, *59*, 187–192. [CrossRef]

47. Prathep, A.; Kaewsrikhaw, R.; Mayakun, J.; Darakrai, A. The effects of light intensity and temperature on the calcification rate of Halimeda macroloba. *J. Appl. Phycol.* **2018**, *30*, 3405–3412. [CrossRef]

48. Diaz-Pulido, G.; Cornwall, C.; Gartrell, P.; Hurd, C.; Tran, D. V Strategies of dissolved inorganic carbon use in macroalgae across a gradient of terrestrial influence: Implications for the Great Barrier Reef in the context of ocean acidification. *Coral Reefs* **2016**, *35*, 1327–1341. [CrossRef]

49. Cornwall, C.E.; Revill, A.T.; Hall-Spencer, J.M.; Milazzo, M.; Raven, J.A.; Hurd, C.L. Inorganic carbon physiology underpins macroalgal responses to elevated CO_2. *Sci. Rep.* **2017**, *7*, srep46297. [CrossRef] [PubMed]

50. Borowitzka, M.A.; Larkum, A.W.D. Calcification in the Green Alga Halimeda: III. The sources of inorganic carbon for photosynthesis and calcification and a model of the mechanism of calcification. *J. Exp. Bot.* **1976**, *27*, 879–893. [CrossRef]

51. Böhm, L.; Fütterer, D.; Kaminski, E. Algal calcification in some Codiaceae (Chlorophyta): Ultrastructure and location of skeletal deposits 1, 2. *J. Phycol.* **1978**, *14*, 486–493. [CrossRef]

52. Mauffrey, A.R.L.; Cappelatti, L.; Griffin, J.N. Seaweed functional diversity revisited: Confronting traditional groups with quantitative traits. *J. Ecol.* **2020**, *108*, 2390–2405. [CrossRef]

53. Jokiel, P.L. Ocean acidification and control of reef coral calcification by boundary layer limitation of proton flux. *Bull. Mar. Sci.* **2011**, *87*, 639–657. [CrossRef]

54. Ries, J.B. A physicochemical framework for interpreting the biological calcification response to CO_2-induced ocean acidification. *Geochim. Cosmochim. Acta* **2011**, *75*, 4053–4064. [CrossRef]

55. Tyler, C.; Kai, S.; Jokiel, P.L. Predicting the impact of ocean acidification on coral reefs: Evaluating the assumptions involved. *ICES J. Mar. Sci.* **2016**, *73*, 550–557. [CrossRef]

56. Frankignoulle, M.; Pichon, M.; Gattuso, J.-P. Aquatic Calcification as a Source of Carbon Dioxide. In *Carbon Sequestration Biosphere*; Springer: Berlin/Heidelberg, Germany, 1995.

57. Semesi, I.S.; Beer, S.; Björk, M. Seagrass photosynthesis controls rates of calcification and photosynthesis of calcareous macroalgae in a tropical seagrass meadow. *Mar. Ecol. Prog. Ser.* **2009**, *382*, 41–47. [CrossRef]

58. Mayakun, J.; Prathep, A. Calcium carbonate productivity by *Halimeda macroloba* in the tropical intertidal ecosystem: The significant contributor to global carbonate budgets. *Phycol. Res.* **2019**, *67*, 94–101. [CrossRef]

59. Mayakun, J.; Liao, C.-P.; Liu, S.-L. The standing stock and $CaCO_3$ contribution of *Halimeda macroloba* in the tropical seagrass-dominated ecosystem in Dongsha Island, the main island of Dongsha Atoll, South China Sea. *J. Mar. Biol. Assoc. United Kingd.* **2020**, *100*, 1219–1227. [CrossRef]

60. Pentecost, A. Calcification Processes in Algae and Cyanobacteria. In *Calcareous Algae and Stromatolites*; Springer: Berlin/Heidelberg, Germany, 1991.

61. Egilsdottir, H.; Olafsson, J.; Martin, S. Photosynthesis and calcification in the articulated coralline alga *Ellisolandia elongata* (Corallinales, Rhodophyta) from intertidal rock pools. *Eur. J. Phycol.* **2016**, *51*, 59–70. [CrossRef]

62. Williamson, C.J.; Perkins, R.; Voller, M.; Yallop, M.L.; Brodie, J. The regulation of coralline algal physiology, an in situ study of *Corallina officinalis* (Corallinales, Rhodophyta). *Biogeosciences* **2017**, *14*, 4485–4498. [CrossRef]

63. Jensen, P.R.; Gibson, R.A.; Littler, M.M.; Littler, D.S. Photosynthesis and calcification in four deep-water Halimeda species (chlorophyceae, caulerpales). *Deep Sea Res. Part A Oceanogr. Res. Pap.* **1985**, *32*, 451–464. [CrossRef]

64. De Beer, D.; Larkum, A.W.D. Photosynthesis and calcification in the calcifying algae *Halimeda discoidea* studied with microsensors. *Plant. Cell Environ.* **2001**, *24*, 1209–1217. [CrossRef]

65. McConnaughey, T.A.; Whelan, J.F. Calcification generates protons for nutrient and bicarbonate uptake. *Earth-Sci. Rev.* **1997**, *42*, 95–117. [CrossRef]

66. Borowitzka, M.A. Morphological and Cytological Aspects of Algal Calcification. In *International Review of Cytology*; Elsevier: Amsterdam, The Netherlands, 1982; pp. 127–162.

67. Hofmann, L.C.; Schoenrock, K.; de Beer, D. Arctic coralline algae elevate surface pH and carbonate in the dark. *Front. Plant Sci.* **2018**, *9*, 1416. [CrossRef]

68. Borowitzka, M.A.; Larkum, A.W.D. Calcification in the green alga *Halimeda*. I. An Ultrastructure study of thallus development 1. *J. Phycol.* **1977**, *13*, 6–16. [CrossRef]

69. Lee, D.; Carpenter, S.J. Isotopic disequilibrium in marine calcareous algae. *Chem. Geol.* **2001**, *172*, 307–329. [CrossRef]

70. Gil-Díaz, T.; Haroun, R.; Tuya, F.; Betancor, S.; Viera-Rodríguez, M.A. Effects of ocean acidification on the brown alga *Padina pavonica*: Decalcification due to acute and chronic events. *PLoS ONE* **2014**, *9*, e108630. [CrossRef]

71. Goffredo, S.; Prada, F.; Caroselli, E.; Capaccioni, B.; Zaccanti, F.; Pasquini, L.; Fantazzini, P.; Fermani, S.; Reggi, M.; Levy, O.; et al. Biomineralization control related to population density under ocean acidification. *Nat. Clim. Chang.* **2014**, *4*, 593–597. [CrossRef]

72. Pettit, L.R.; Smart, C.W.; Hart, M.B.; Milazzo, M.; Hall-Spencer, J.M. Seaweed fails to prevent ocean acidification impact on foraminifera along a shallow-water CO_2 gradient. *Ecol. Evol.* **2015**, *5*, 1784–1793. [CrossRef]

73. Betancor, S.; Tuya, F.; Gil-Díaz, T.; Figueroa, F.L.; Haroun, R. Effects of a submarine eruption on the performance of two brown seaweeds. *J. Sea Res.* **2014**, *87*, 68–78. [CrossRef]

74. Celis-Plá, P.S.M.; Hall-Spencer, J.M.; Horta, P.A.; Milazzo, M.; Korbee, N.; Cornwall, C.E.; Figueroa, F.L. Macroalgal responses to ocean acidification depend on nutrient and light levels. *Front. Mar. Sci.* **2015**, *2*, 26. [CrossRef]

75. Vogel, N.; Fabricius, K.E.; Strahl, J.; Noonan, S.H.C.; Wild, C.; Uthicke, S. Calcareous green alga *Halimeda* tolerates ocean acidification conditions at tropical carbon dioxide seeps. *Limnol. Oceanogr.* **2015**, *60*, 263–275. [CrossRef]

76. Price, N.; Hamilton, S.; Tootell, J.; Smith, J. Species-specific consequences of ocean acidification for the calcareous tropical green algae Halimeda. *Mar. Ecol. Prog. Ser.* **2011**, *440*, 67–78. [CrossRef]

77. Schubert, N.; Hofmann, L.C.; Almeida Saá, A.C.; Moreira, A.C.; Arenhart, R.G.; Fernandes, C.P.; de Beer, D.; Horta, P.A.; Silva, J. Calcification in free-living coralline algae is strongly influenced by morphology: Implications for susceptibility to ocean acidification. *Sci. Rep.* **2021**, *11*, 11232. [CrossRef]

78. Borowitzka, M.A. Mechanism in algal calcification. *Prog. Phycol. Res.* **1982**, *1*, 137–177.

79. Ralph, P.J.; Gademann, R. Rapid light curves: A powerful tool to assess photosynthetic activity. *Aquat. Bot.* **2005**, *82*, 222–237. [CrossRef]

80. Schneider, C.A.; Rasband, W.S.; Eliceiri, K.W. NIH Image to ImageJ: 25 years of image analysis. *Nat. Methods* **2012**, *9*, 671–675. [CrossRef] [PubMed]

81. Cappelatti, L.; Mauffrey, A.R.L.; Griffin, J.N. Applying continuous functional traits to large brown macroalgae: Variation across tidal emersion and wave exposure gradients. *Mar. Biol.* **2019**, *166*, 145. [CrossRef]

82. Pierrot, D.; Lewis, E.; Wallace, D.W.R. MS Excel Program Developed for CO_2 System Calculations: ORNL/CDIAC-105a. Carbon Dioxide Information Analysis Center, Oak Ridge National Laboratory, U.S. Department of Energy, Oak Ridge, Tennessee. 2006. Available online: http://marine.gov.scot/sma/content/ms-excel-program-developed-co2-system-calculations (accessed on 21 October 2021).

83. Smith, S.V.; Key, G.S. Carbon dioxide and metabolism in marine environments1. *Limnol. Oceanogr.* **1975**, *20*, 493–495. [CrossRef]

84. Gazeau, F.; Quiblier, C.; Jansen, J.M.; Gattuso, J.-P.; Middelburg, J.J.; Heip, C.H.R. Impact of elevated CO_2 on shellfish calcification. *Geophys. Res. Lett.* **2007**, *34*, L07603. [CrossRef]

85. Haynes, D.; Ralph, P.; Prange, J.; Dennison, B. The Impact of the herbicide Diuron on photosynthesis in three species of tropical Seagrass. *Mar. Pollut. Bull.* **2000**, *41*, 288–293. [CrossRef]

86. Laurent, J.; Tambutté, S.; Tambutté, É.; Allemand, D.; Venn, A. The influence of photosynthesis on host intracellular pH in scleractinian corals. *J. Exp. Biol.* **2012**, *216*, 1398–1404. [CrossRef]